

Molecular identification of Ca²⁺-activated K⁺ channels in parotid acinar cells

Keith Nehrke, Claire C. Quinn and Ted Begenisich

Am J Physiol Cell Physiol 284:535-546, 2003. First published Oct 16, 2002;

doi:10.1152/ajpcell.00044.2002

You might find this additional information useful...

This article cites 38 articles, 21 of which you can access free at:

<http://ajpcell.physiology.org/cgi/content/full/284/2/C535#BIBL>

This article has been cited by 12 other HighWire hosted articles, the first 5 are:

The role of cell cholesterol and the cytoskeleton in the interaction between IK1 and maxi-K channels

V. G. Romanenko, K. S. Roser, J. E. Melvin and T. Begenisich

Am J Physiol Cell Physiol, April 1, 2009; 296 (4): C878-C888.

[Abstract] [Full Text] [PDF]

Activation of Stretch-Activated Channels and Maxi-K⁺ Channels by Membrane Stress of Human Lamina Cribrosa Cells

M. Irnaten, R. C. Barry, B. Quill, A. F. Clark, B. J. P. Harvey and C. J. O'Brien

Invest. Ophthalmol. Vis. Sci., January 1, 2009; 50 (1): 194-202.

[Abstract] [Full Text] [PDF]

Physiology and Pathophysiology of Potassium Channels in Gastrointestinal Epithelia

D. Heitzmann and R. Warth

Physiol Rev, July 1, 2008; 88 (3): 1119-1182.

[Abstract] [Full Text] [PDF]

Apical maxi-K (KCa1.1) channels mediate K⁺ secretion by the mouse submandibular exocrine gland

T. Nakamoto, V. G. Romanenko, A. Takahashi, T. Begenisich and J. E. Melvin

Am J Physiol Cell Physiol, March 1, 2008; 294 (3): C810-C819.

[Abstract] [Full Text] [PDF]

Regulation of membrane potential and fluid secretion by Ca²⁺-activated K⁺ channels in mouse submandibular glands

V. G. Romanenko, T. Nakamoto, A. Srivastava, T. Begenisich and J. E. Melvin

J. Physiol., June 1, 2007; 581 (2): 801-817.

[Abstract] [Full Text] [PDF]

Updated information and services including high-resolution figures, can be found at:

<http://ajpcell.physiology.org/cgi/content/full/284/2/C535>

Additional material and information about *AJP - Cell Physiology* can be found at:

<http://www.the-aps.org/publications/ajpcell>

This information is current as of July 6, 2009 .

Molecular identification of Ca²⁺-activated K⁺ channels in parotid acinar cells

KEITH NEHRKE,^{1,*} CLAIRE C. QUINN,^{1,*} AND TED BEGENISICH²

¹Center for Oral Biology, Aab Institute of Biomedical Sciences, and ²Department of Pharmacology and Physiology, University of Rochester Medical Center, Rochester, New York 14642

Submitted 29 January 2002; accepted in final form 15 October 2002

Nehrke, Keith, Claire C. Quinn, and Ted Begenisich. Molecular identification of Ca²⁺-activated K⁺ channels in parotid acinar cells. *Am J Physiol Cell Physiol* 284: C535–C546, 2003. First published October 16, 2002; 10.1152/ajpcell.00044.2002.—We used molecular biological and patch-clamp techniques to identify the Ca²⁺-activated K⁺ channel genes in mouse parotid acinar cells. Two types of K⁺ channels were activated by intracellular Ca²⁺ with single-channel conductance values of 22 and 140 pS (in 135 mM external K⁺), consistent with the intermediate and maxi-K classes of Ca²⁺-activated K⁺ channels, typified by the mIK1 (*Kcnn4*) and mSlo (*Kcnma1*) genes, respectively. The presence of mIK1 mRNA was established in acinar cells by in situ hybridization. The electrophysiological and pharmacological properties of heterologously expressed mIK1 channels matched those of the native current; thus the native, smaller conductance channel is likely derived from the mIK1 gene. We found that parotid acinar cells express a single, uncommon splice variant of the mSlo gene and that heterologously expressed channels of this Slo variant had a single-channel conductance indistinguishable from that of the native, large-conductance channel. However, the sensitivity of this expressed Slo variant to the scorpion toxin iberiotoxin was considerably different from that of the native current. RT-PCR analysis revealed the presence of two mSlo β -subunits (*Kcnmb1* and *Kcnmb4*) in parotid tissue. Comparison of the iberiotoxin sensitivity of the native current with that of parotid mSlo expressed with each β -subunit in isolation and measurements of the iberiotoxin sensitivity of currents in cells from β_1 knockout mice suggest that parotid acinar cells contain approximately equal numbers of homotetrameric channel proteins from the parotid variant of the Slo gene and heteromeric proteins composed of the parotid Slo variant in combination with the β_4 -subunit.

secretory cells; fluid secretion; single channels; patch clamp

SALIVARY GLAND SECRETION plays an extremely important role in maintaining the health of oral tissues. The fluid secretion hydrates the oral cavity, aiding in the mastication and swallowing of food. In addition, these secretions neutralize acids and protect against the invasion of potential pathogens. An increase in intracellular Ca²⁺, usually associated with muscarinic receptor stimulation, triggers fluid secretion by simulta-

neously activating apical Cl⁻ channels and basolateral K⁺ channels. Indeed, nonselective K⁺ channel blockers inhibit fluid secretion and Cl⁻ efflux (19, 21). The efflux of Cl⁻ and K⁺ across the apical and basolateral membranes, respectively, produces a transepithelial potential difference that draws Na⁺ through tight junctions into the lumen. The resulting transepithelial osmotic gradient drives the movement of water, creating a plasma-like primary secretion.

The presence of several types of Ca²⁺-activated cation channels in salivary acinar cells has been reported. These include a K⁺ channel with a large single-channel conductance near 160 pS in both rodents (22) and humans (23, 29), a 15-pS channel permeable to Na⁺ (22) in humans, a 30-pS Na⁺-permeable channel in rodents (22), a 30-pS K⁺-selective channel in humans, and a 40-pS K⁺ channel in mice (14). The variety of channel types in different tissues and species and the lack of any specific information on the genes that code for these channels complicate efforts to understand the roles of these various channels in fluid secretion.

As a first step toward an understanding of the role of K⁺ channels in salivary function, we designed an approach to determine the molecular identities of the Ca²⁺-activated K⁺ channels in the mouse model system. Patch-clamp analysis of currents from mouse parotid acinar cells revealed two levels of single-channel current that were activated by increases in intracellular Ca²⁺. On the basis of the expression profile of channel mRNA in parotid acinar cells, in combination with the electrical and pharmacological properties of native and recombinantly expressed channels, the native, small-conductance channel is likely derived from the mIK1 gene. The larger conductance channel likely reflects expression of a single “insertless” splice variant of the mSlo gene. Northern blot analysis revealed the expression of two mSlo β -subunits in mouse parotid tissue. We compared the iberiotoxin sensitivity of the channels in native tissue with heterologously expressed channels containing each β -subunit. These results and the toxin sensitivity of channels from parotid acinar cells of a β_1 knockout mouse suggest that ~50% of the native maxi-K channels are homotetramers of

*K. Nehrke and C. C. Quinn contributed equally to this work.

Address for reprint requests and other correspondence: T. Begenisich, Dept. of Pharmacology and Physiology, Box 711, Univ. of Rochester Medical Center, Rochester, NY 14642 (E-mail: ted_begenisich@urmc.rochester.edu).

The costs of publication of this article were defrayed in part by the payment of page charges. The article must therefore be hereby marked “advertisement” in accordance with 18 U.S.C. Section 1734 solely to indicate this fact.

the parotid mSlo splice variant and that the remaining large-conductance channels are heteromeric proteins from this mSlo variant complexed with the β_4 -subunit.

MATERIALS AND METHODS

Western analysis. Mouse brain and parotid homogenates were used to identify native maxi-K channel protein. Tissues were prepared as previously described (34). After dissection, the tissues were homogenized twice by 10-s strokes at power level 5 with a Polytron homogenizer (Brinkmann Instruments, Westbury, NY) in 5 ml of homogenization solution (10 mM HEPES adjusted to pH 7.4 with Tris, 10% sucrose, 1 mM EDTA, and 1 mM PMSF) per gram of tissue, with 1 tablet of Complete protease inhibitor (Roche Applied Science, Indianapolis, IN) per 50 ml. Homogenates were centrifuged at 2,500 g for 15 min at 4°C, and the supernatants were saved. The pellets were resuspended in 5 ml of homogenization buffer per gram of starting tissue and then homogenized and recentrifuged as described above. The supernatants were combined, and crude membrane proteins were precipitated by centrifugation at 22,000 g for 20 min at 4°C. The supernatants from this step were discarded, and the pellets were resuspended in PBS containing 1 mM EDTA, 1 mM PMSF, and Complete protease inhibitor (1 tablet per 50 ml) and then passed once through a 25-gauge needle and once through a 30-gauge needle. Aliquots were quickly frozen in liquid N₂ and stored at -85°C until use.

Approximately 20 μ g of crude membrane protein were separated by two-phase Tricine polyacrylamide gel electrophoresis (10% T/6% C resolving layer, 4% T/3% C stacking layer) and transferred onto nitrocellulose membrane (Hybond ECL; Amersham Pharmacia Biotech, Piscataway, NJ) in buffer containing 10 mM 3-(cyclohexylamino)-1-propane-sulfonic acid (CAPS) adjusted to pH 11 and 10% methanol. The blot was blocked overnight at room temperature in blocking buffer (PBS containing 1% Tween 20, 4% BSA, and 1% normal goat serum). After blocking, the blot was incubated for 2 h at room temperature in blocking buffer containing a 1:250 dilution of rabbit anti-mSlo polyclonal antibody (Alomone Laboratories, Jerusalem, Israel), washed three times with PBS-T (PBS containing 1% Tween 20), incubated for 1 h at room temperature in blocking buffer containing a 1:5,000 dilution of horseradish peroxidase-conjugated goat anti-rabbit IgG (Jackson ImmunoResearch Laboratories, West Grove, PA), and again washed three times with PBS-T. Immune complexes were detected on film using Enhanced ChemiLuminescence (ECL; Amersham Pharmacia Biotech).

Northern blot analysis, in situ hybridization, and RT-PCR. Total RNA was prepared using Trizol reagent (Life Technologies, Grand Island, NY) according to the manufacturer's instructions. mRNA was further purified by chromatography on oligo(dT) resin. The RNA was fractionated by electrophoresis in a formaldehyde-agarose gel and transferred to Hybond-XL nylon membrane (Amersham). The blot was hybridized with a ³²P-labeled double-stranded probe generated from nucleotides 96–519 of the mIK1 cDNA, nucleotides 1347–3591 of the mSlo cDNA, or the entire coding region of the β_1 or β_4 cDNAs in ExpressHyb solution (Clontech, Palo Alto, CA) as recommended by the manufacturer.

A subclone containing nucleotides 907–1467 of the mIK1 cDNA (start codon at base 41) was used for in situ hybridization analysis. In situ hybridization with the antisense cRNA probe was performed using a modification of procedures described by Wilkinson and Green (38). Mouse parotid gland was fixed overnight in freshly prepared ice-cold 4% paraformaldehyde in PBS. The gland was dehydrated

through ethanol into xylene and embedded in paraffin using a Tissue-Tek V.I.P. automatic processor (Miles, Mishawaka, IN). Sections (5 μ m) were adhered to commercially modified glass slides (Superfrost Plus; VWR, Rochester, NY), dewaxed in xylene, rehydrated through graded ethanols, and treated with proteinase K to enhance probe accessibility and with acetic anhydride to reduce nonspecific background. Single-stranded RNA probes were prepared by standard techniques with specific activities of 5×10^9 dpm/mg. Sections were hybridized at 15°C below the melting temperature, washed at high stringency (7°C below melting temperature), and treated with RNase A to further diminish nonspecific adherence of the probe. Autoradiography with NBT-2 emulsion (Eastman Kodak, Rochester, NY) was performed for 25 days. Slides were developed with D19 (Eastman Kodak), and the tissue was counterstained with hematoxylin. Bright-field and dark-field images were captured with a Polaroid Digital Microscope camera (Cambridge, MA) and processed using Adobe Photoshop with Image Processing Toolkit (Reindeer Games, Asheville, NC).

For RT-PCR analysis, 1 μ g of total RNA was used to synthesize first-strand cDNA by using an RT-PCR kit (Clontech) according to the manufacturer's protocol. PCR reactions were annealed at 7°C below the melting temperature and run for the indicated number of cycles. Oligonucleotide pairs for amplification of mSlo1, -2, and -3 (*Kcnma1-3* gene products) were designed against nucleotides 1775–2066 of the mSlo1 coding region, nucleotides 1–353 of the mouse expressed sequence tag (EST) BE655597, which presumably codes for mSlo2 (Slack), a mouse homolog of the *Caenorhabditis elegans* Slo-2 protein (39), and nucleotides 1873–2137 of mSlo-3. Oligonucleotide pairs for amplification of the mSlo β -subunits 1 through 4 (*Kcnmb1-4* gene products) were designed on the basis of the published sequence of the mouse β_1 (nucleotides 198–426 of the open reading frame) and β_4 (nucleotides 224–465 of the open reading frame) subunits and the published sequence of the human β_2 (nucleotides 310–543 of the open reading frame) and β_3 (nucleotides 279–519 of the open reading frame) subunits. Although the products amplified in parentheses above code for regions that are conserved among the β -subunits, the oligonucleotide pairs do not cross-hybridize. The efficacy of the β_2 and β_3 primers was assessed by using a mouse tissue control known to be positive for those subunits (see text). All PCR bands of an inappropriate size were cloned and sequenced and were found to be the result of nonspecific amplification of unrelated gene products.

Cloning strategies. Parotid mSlo splice-site variation was analyzed by sequencing RT-PCR products amplified from mouse parotid gland first-strand cDNA. For clarity, all nucleotide designations refer back to the first published mSlo coding sequence (accession no. L16912; Ref. 8). Our analysis proceeded in three steps. First, we sequenced more than 20 clones from the COOH-terminal coding region containing nucleotides 1775–3591, where much of the splice-site variation occurs. Next, we used 5'-RACE (rapid amplification of cDNA ends) to determine the start codon, again sequencing multiple clones. Finally, we amplified the full-length open reading frame and examined the sequences coding for the transmembrane domains. This analysis suggested the presence of a single parotid mSlo variant (which we have called "parSlo" to unambiguously distinguish this from the common mSlo splice variant) that had no insertions at any of the characterized mSlo splice sites 1–6 (accession no. AF465344). Compared with mSlo, parSlo lacks 1) the first 81 bases, which results in the use of the "M1" alternative start codon; 2) nucleotides 1979–1987 at splice site 4, located between the

eighth and ninth putative membrane-spanning segments; and 3) nucleotides 3408–3436 at splice site 6, which shifts the reading frame, resulting in the use of a cryptic stop codon and the formation of a “short” protein.

To clone parSlo for expression studies, we used PCR to amplify a region spanning nucleotides 776–3591 by using a *NotI*-tagged 3′ primer and a mouse parotid cDNA template. An *SphI-NotI* fragment containing nucleotides 1347–3591 was then digested from the PCR product and cloned into the complementary sites in a vector containing an mSlo variant that is identical to parSlo from the start codon to nucleotide 1347 (8). The entire coding sequence was then digested from the resulting vector and subcloned into pcDNA3.1 (Invitrogen, Carlsbad, CA) using *KpnI* and *XbaI*.

The β_1 - and the β_4 -subunit coding regions were amplified from first-strand parotid cDNA by using oligonucleotides that included the start and stop codons and that had been tagged with a Kozak translation initiation sequence and *NheI-BglII* restriction sites. The resulting PCR products were then cloned into the complementary sites of the vector pIRES2-EGFP (Clontech). The mIK1 coding sequence was similarly amplified from first-strand cDNA by using tagged primer pairs and was cloned into the *NheI-BglII* sites of pIRES2-EGFP. The full coding sequences of all of the PCR-generated clones were sequenced on both strands to ensure fidelity.

Cell transfection. Chinese hamster ovary (CHO) cells and TSA cells [human embryonic kidney (HEK)-293 cells stably transfected with the large T antigen, provided by Ronald Li and Eduardo Marban, Johns Hopkins University, Baltimore, MD] were cultured in DMEM plus 10% newborn calf serum and antibiotics in a 5% CO₂ incubator at 37°C. Before transfection, cells were plated onto 100-mm culture dishes and grown to ~70% confluency and then transfected with a total of 10 μ g of DNA per dish by using Superfect transfection reagent (Qiagen) following the manufacturer’s recommended protocol. The mIK construct was subcloned into the pIRES2-EGFP vector, which allowed identification of transfected cells with fluorescence microscopy. The parotid mSlo variant (in pcDNA3.1) was expressed in a 1:1 ratio with the pIRES2-EGFP vector. The β_1 - or β_4 -subunits (in pIRES2-EGFP) were cotransfected with parSlo (pcDNA3.1) in a 4:1 ratio.

Electrophysiological methods. Single acinar cells were dissociated from mouse parotid glands with a modification of the methods previously used for rats (1). Briefly, glands were dissected from exsanguinated mice after CO₂ anesthesia. Unless otherwise indicated, the data presented here are from BlackSwiss \times 129/SvJ hybrid mice. In addition, we also used β_1 knockout mice (7), kindly provided by R. Brenner and R. W. Aldrich (Department of Molecular and Cellular Physiology, Stanford University School of Medicine, Stanford, CA), and mice (C57BL/6J) that are the wild-type “controls” for the β_1 knockout animals. Glands were minced in Ca²⁺-free minimum essential medium (MEM; GIBCO BRL, Gaithersburg, MD) supplemented with 1% BSA (fraction V; Sigma Chemical, St. Louis, MO). The tissue was treated for 20 min (37°C) with a 0.02% trypsin solution (MEM-Ca²⁺ free + 1 mM EDTA + 2 mM glutamine + 1% BSA). Digestion was stopped with 2 mg/ml soybean trypsin inhibitor (Sigma Chemical), and the tissue was further dispersed by two sequential 60-min treatments with collagenase (100 U/ml type CLSPA; Worthington Biochemical, Freehold, NJ) in MEM-Ca²⁺ free plus 2 mM glutamine plus 1% BSA. The dispersed cells were centrifuged and washed with basal medium Eagle (BME) (GIBCO)/BSA free. The final pellet was resuspended in BME/BSA free plus 2 mM glutamine, and

cells were plated onto poly-L-lysine-coated glass coverslips for electrophysiological recordings.

Whole cell and single-channel patch-clamp recordings were done at room temperature (20–22°C) with an Axopatch 1-D amplifier (Axon Instruments, Foster City, CA). Data acquisition was performed by using a 12-bit analog-to-digital converter controlled by a personal computer. Whole cell K⁺ channel currents were measured from native parotid acinar cells and from HEK and CHO cells transfected with various channel clones. Except where indicated, we used an internal solution that consisted of 135 mM K-glutamate, 10 mM HEPES (pH 7.2), and various free Ca²⁺ concentrations established by an EGTA-Ca buffer system with 5 mM total EGTA (Ref. 5; see also <http://www.stanford.edu/~cpatton/maxc.html>). The external solution consisted of (in mM) 135 Na-glutamate, 5 K-glutamate, 2 CaCl₂, 2 MgCl₂, and 10 HEPES, pH 7.2.

We measured single-channel currents from both on-cell and excised, inside-out patches of parotid acinar cells. Ca²⁺-activated currents were stimulated in on-cell patches by application of 5 μ M carbachol and in excised patches by application of the 135 K-glutamate internal solution with buffered Ca²⁺ levels to the inside surface of the patch. The cell membrane voltage was nulled with an isotonic K-glutamate solution. The external (pipette) solution for both on-cell and excised patches contained (in mM) 135 K-glutamate, 2 CaCl₂, 2 MgCl₂, and 10 HEPES (pH 7.2). Long stretches of data containing openings of one to three single channels were selected for determining amplitude histograms. These were fit with a Gaussian function to determine the single-channel current levels.

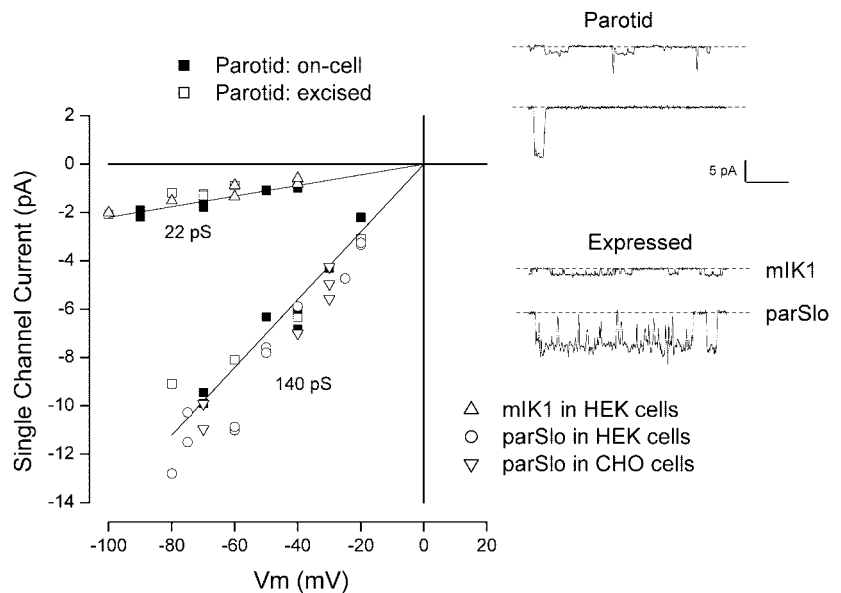
We examined the dose dependence of block of current by several pharmacological compounds. We determined the EC₅₀ values for these compounds by a nonlinear least-squares fit of the standard binding isotherm to the data in the Origin software of the OriginLab (Northampton, MA). The error limits on the EC₅₀ values are the estimated standard errors of this parameter provided by the software.

Iberitoxin (IBX) and clotrimazole were purchased from Sigma, and paxilline was from Biomol (Plymouth Meeting, PA). Charybdotoxin (CTX) was produced by expressing and purifying a cleavable fusion protein in *Escherichia coli* (28, 32). All solutions in experiments with IBX and CTX included 30 μ g/ml BSA.

RESULTS

Fluid secretion in parotid acinar cells is stimulated by muscarinic agonists that mobilize intracellular Ca²⁺. This process involves the activation of both Ca²⁺-activated Cl⁻ and Ca²⁺-activated K⁺ channels. We found significant activity of only two types of single K⁺ channel currents in on-cell patches of mouse parotid acinar cells stimulated by 5 μ M of the secretagogue carbachol. Examples of these currents are shown in Fig. 1, *top inset*. When the currents from on-cell patches were recorded with an extracellular K⁺ concentration of 135 mM, the two levels were near 22 and 140 pS (Fig. 1, filled squares). These same two levels of conductance were observed from patches excised into Ca²⁺-containing intracellular solutions (Fig. 1, open squares). Of eight patches, five contained both channel types, two contained openings only of the small-conductance level, and one had openings of only the large-conductance channel. The amplitude histograms (see

Fig. 1. Single-channel currents from native parotid acinar cells and from cells expressing mIK1 and parSlo. Single-channel current-voltage relationships are shown for large- and small-conductance channels recorded from on-cell patches of parotid acinar cells (■); excised, inside-out patches from acinar cells (□); inside-out patches from HEK cells transfected with mIK1 (△); inside-out patches from human embryonic kidney (HEK) cells transfected with parSlo (○); and inside-out patches from Chinese hamster ovary (CHO) cells transfected with parSlo (▽). For the on-cell patches, channels were activated with 5 μ M carbachol. Channels in excised patches were activated by 160, 300, or 400 nM Ca²⁺. *Inset*: examples of the small- and large-conductance channels observed in on-cell patches on parotid acinar cells recorded at -70 mV (*top*) and examples of currents from inside-out patches from HEK cells transfected with mIK1 and parSlo channels and recorded at -80 and -75 mV, respectively (*bottom*). Calibration: 5 pA for all records and 20 ms for parotid channels and mSlo, 100 ms for mIK1.



Electrophysiological methods) showed no signs of sub-conductance states.

These conductance levels suggest that the Ca²⁺-activated K⁺ channels in mouse parotid acinar cells are members of the intermediate and maxi-K families, respectively. Because the intermediate-conductance K⁺ channels are not voltage or time dependent (15, 20, 36, 37) and maxi-K channels are voltage and time dependent (13), the presence of both classes of these channels in parotid acinar cells predicts that the whole cell currents would have two Ca²⁺-dependent components: one that is time and voltage independent and one that is time and voltage dependent. Figure 2 shows that parotid acinar cells do indeed have both these components.

Figure 2A, *inset*, shows whole cell currents recorded from a parotid acinar cell patched with an internal Ca²⁺ concentration of 160 nM. Shown are currents in response to steps of membrane voltage to -110, -30, +10, and +50 mV from a holding potential of -70 mV. Steps to negative voltages elicited currents with little time dependence (after the capacitive current transient), whereas strong depolarizations produced currents in a time- and voltage-dependent manner. The voltage dependence of the current measured at the end of the 40-ms pulses is shown in the main part of Fig. 2A. The current-voltage relationship can be seen to contain two components: a linear one at potentials more negative than about -50 mV, and an outward rectifying component at positive potentials. The broken line represents a linear fit to the current at the four most negative potentials. The interpolated zero-current potential was -78 mV, which is close to the expected K⁺ equilibrium potential of -82 mV for the solutions used in this experiment. Thus the Ca²⁺-activated current in mouse parotid acinar cells is consistent with the expression of both intermediate-conductance and maxi-K channels.

Intermediate-conductance K⁺ channels have a high sensitivity to the antifungal agent clotrimazole (15, 20,

36, 37). Maxi-K channels are generally resistant to this agent (39). Thus, if these two types of channels are expressed in parotid acinar cells, the linear, time-independent component should be inhibited by clotrimazole with little or no effect on the nonlinear, time-dependent current. Figure 2B shows that the addition of 300 nM clotrimazole to the cell shown in Fig. 2A inhibited the linear component by ~70% with no clear effect on the time-dependent, nonlinear current. The average inhibition of the linear component by 300 nM clotrimazole was $78 \pm 2.8\%$ (mean \pm SE, $n = 4$). Current block in several similar experiments with a range of clotrimazole concentrations was consistent with an EC₅₀ value of 30 ± 5.5 nM.

Thus mIK1 represents a reasonable candidate for the time- and voltage-insensitive Ca²⁺-activated K⁺ channel in parotid acinar cells. The human IK isoform, hIK1, has been shown via a multiple tissue RNA dot blot to be highly expressed in salivary glands as well as in several other nonexcitable tissues (17). Northern blot analysis of mouse tissues with the use of a probe complementary to the 5' portion of mIK1 detected a single transcript of ~2.2 kb in both colon and parotid gland, consistent with the expected size of the mIK1 message (Fig. 3A). Subsequent *in situ* hybridization of semi-thin parotid gland sections with an antisense cRNA suggested that mIK1 expression is limited to the acinar cells and does not occur in cells of the salivary ducts (Fig. 3B). Hybridization with a sense control produced only a weak and nonspecific signal (data not shown).

To solidify the identification of mIK1 as the time- and voltage-independent Ca²⁺-activated K⁺ channel in parotid acinar cells, we compared several properties of mIK1 expressed in HEK cells with the currents in the native cells. An example of single-channel currents in an excised inside-out patch from a HEK cell transfected with mIK1 is shown in Fig. 1, *bottom inset*. The current-voltage relationship of single, expressed mIK1 channels (Fig. 1, open triangles) was indistinguishable

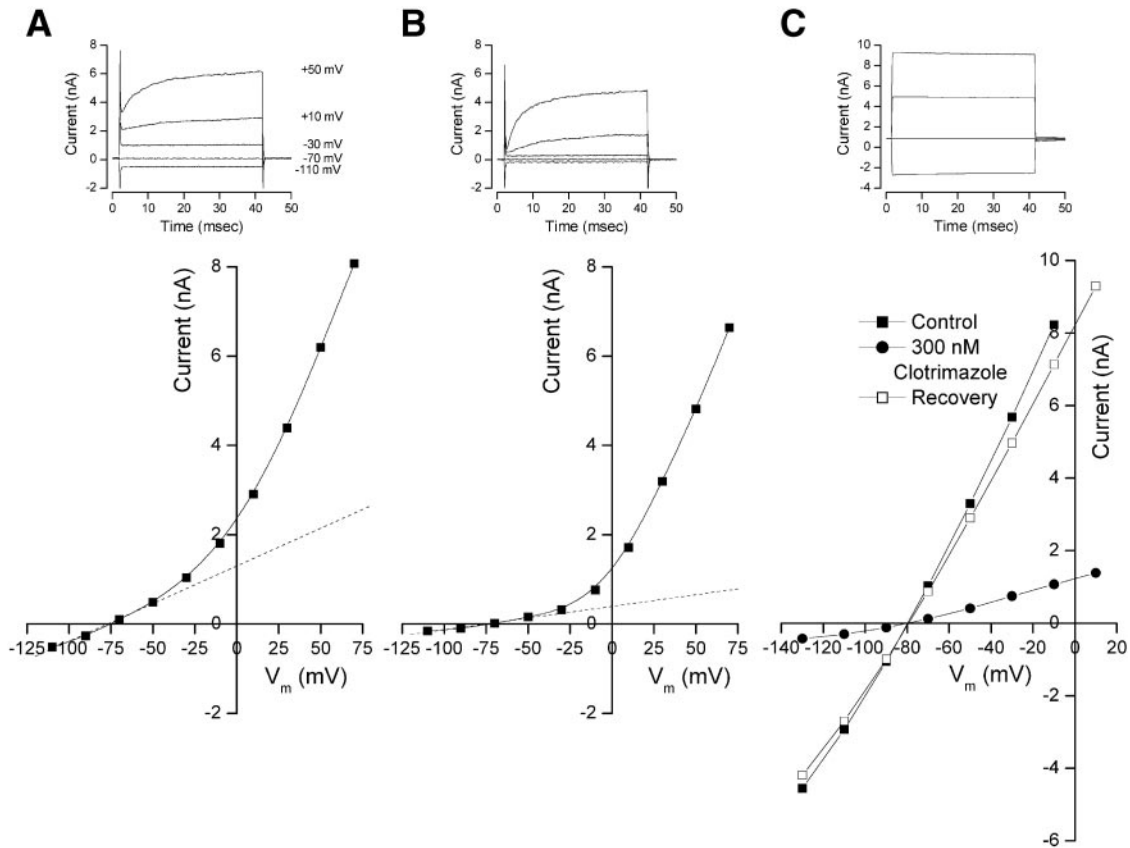


Fig. 2. Comparison of time- and voltage-independent K⁺ current in native cells with expressed mIK1. *A, inset:* raw currents from a parotid acinar cell in response to step changes in the membrane voltage from a -70-mV holding potential to the indicated values. Main graph in *A* shows currents measured at the end of the test pulses (■) to the indicated membrane potentials (V_m). Dotted line represents linear least-squares fit to the 4 most negative voltages. *B:* data from the same cell as in *A* in the presence of 300 nM clotrimazole. *C, inset:* raw currents from a HEK cell transfected with mIK1. Main graph in *C* shows current-voltage relationship of expressed mIK1 current before (■), during (●), and after washout (□) of 300 nM clotrimazole.

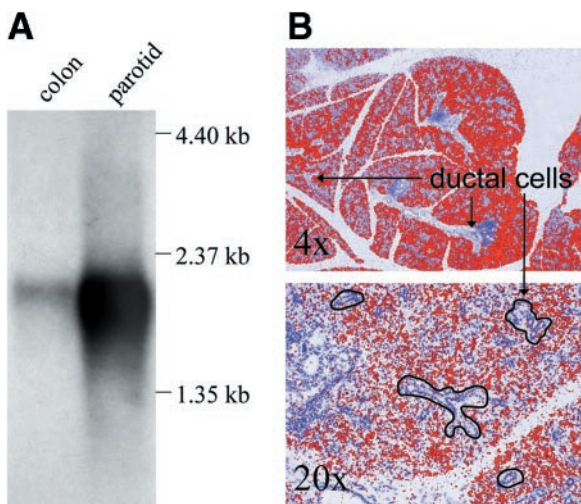


Fig. 3. Northern blot and in situ analysis of parotid mRNA. *A:* Northern analysis of RNA isolated from parotid gland and from colon (as a control) reveals a single transcript of ~2.2 kb. *B:* in situ analysis. Parotid glands were fixed and sectioned at 5 μ M and then probed with an anti-sense mIK1 cRNA. Labeling (red) occurs in the acinar but not ductal cells (outlined in black at $\times 20$ magnification).

from the native, small-conductance channels. Figure 2*C, inset*, shows that expressed mIK1 had little voltage and time dependence, and the main part of Fig. 2*C* shows that expressed mIK1 channels were quite sensitive to 300 nM clotrimazole. Several similar experiments with a range of clotrimazole concentrations were consistent with inhibition of recombinantly expressed mIK1 channel by this compound with an EC_{50} of 18 ± 5 nM, a value a bit smaller than that for the linear component of native cells.

We also compared the tetraethylammonium (TEA) sensitivity of the linear component of native cell current to that of heterologously expressed mIK1 channels. The native current was inhibited by TEA with an EC_{50} value of 6 ± 1 mM. Current through expressed mIK1 channels was inhibited with a similar EC_{50} value of 8.7 ± 1 mM (data not shown).

Thus we found mIK1 to be robustly expressed in mouse parotid acinar cells, and many properties of expressed mIK1 channels were quite similar to those of the linear, Ca²⁺-activated K⁺ current in native cells. We used a similar approach to test the possibility that a product of the Slo gene underlies the time- and voltage-dependent Ca²⁺-activated current in mouse parotid acinar cells.

The Slo1 channel was originally cloned from *Drosophila* (2) and subsequently from mouse and human sources (8, 33). Alternative splicing of the Slo1 gene product in mice (*Kcnma1* gene) and humans (*KCNMA1* gene) results in multiple variants with distinct expression patterns and calcium sensitivities (4, 8, 18, 31). Furthermore, two additional Slo isoforms are encoded by separate genes. Slo2 was first isolated from *C. elegans* and is sensitive to chloride as well as calcium (40), whereas Slo3 expression is restricted to the testes in mice and humans and is insensitive to calcium but sensitive to intracellular pH (30). Both Slo2 and Slo3 homologs can be found in the human genome database of predicted coding regions and in the mouse EST database. RT-PCR analysis of Slo isoforms in mouse parotid gland revealed that expression was limited to the mSlo1 isoform; the amplification of products of the predicted size from kidney and testes cDNA confirmed the efficacy of the mSlo 2 and 3 primer pairs, respectively (Fig. 4). The presence of mSlo was tested for directly by performing Northern and Western blot analyses of parotid gland mRNA and membrane proteins, respectively (Fig. 4, B and C). A single transcript

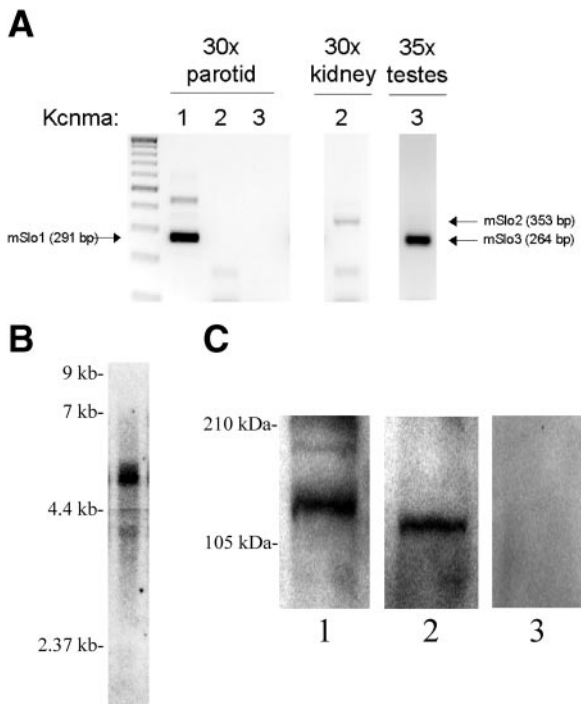


Fig. 4. Expression of mSlo-1, -2, and -3 (*Kcnma1-3* genes) in the parotid gland. **A**: RT-PCR was used to amplify mouse parotid gland cDNA with oligonucleotide pairs specific for the mouse large-conductance Ca²⁺-activated K⁺ channel isoforms 1, 2, and 3 for the indicated number of cycles. mSlo1 was expressed in the parotid gland, whereas mSlo2 and 3 were not. Control reactions indicated that isoforms 2 and 3 were expressed in the kidney and testes, respectively. **B**: Northern blot of parotid mRNA hybridized to a probe for mSlo. The probe detected a band of ~5.3 kb, as expected. **C**: Western blot of brain (lane 1) and parotid (lane 2) membrane proteins with anti-mSlo antibody (Alamone Laboratories). A band of ~115 kDa was detected in both preparations, though the protein from brain appeared to be slightly larger, as predicted from cDNA splice site analysis. Preincubation with a peptide containing the antibody recognition sequence abolished the signal (lane 3).

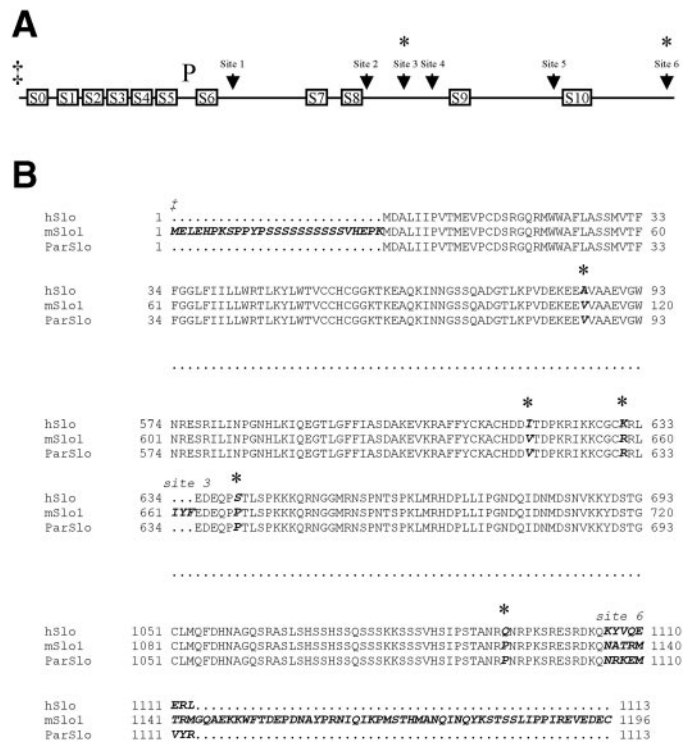


Fig. 5. Splice sites in the mSlo gene. **A**: schematic of the mSlo coding region and splice sites. Putative transmembrane domains S1–S10 are indicated by boxes, characterized splice sites 1–6 are indicated by arrows, and the pore region is denoted as P. The NH₂ terminus of the protein (†) is predicted to be highly diverse based on 5' RACE (8). The splice sites that were found to be altered in the parSlo variant are indicated by an asterisk **B**: sequence alignment of hSlo (GenBank accession no. NM_002247), mSlo (accession no. L16912), and parSlo (accession no. AF465244), the parotid mSlo splice variant. Portions of the proteins that were left out of the alignment and are shown only as dotted lines. The regions where these proteins differ are indicated in bold, with the particular splice sites responsible for the changes noted. Single site differences between hSlo and parSlo are also highlighted by an asterisk. The major differences between mSlo and parSlo consisted of a shorter amino terminus, the absence of the IYF motif at splice site 3, and a retained exon at splice site 6 that contains a premature stop site.

of ~5.3 kb was recognized by an mSlo-specific cDNA probe (Fig. 4B), whereas a commercially available anti-mSlo antibody reacted with a protein with an apparent molecular mass of 115 kDa in both brain and parotid membrane preparations (Fig. 4C). The brain mSlo protein appeared to be slightly larger than the parotid version, consistent with the splice variation that we observed in the parotid gland (see below). Preincubation of the antibody with a purified peptide consisting of the mSlo recognition site resulted in a loss of mSlo-specific signal. Finally, in situ analysis of parotid sections failed to detect mSlo (data not shown), suggesting that the message may be expressed at levels below the detection sensitivity of this method.

Alternative splicing of the Slo channel transcript results in a molecular diversity that can alter the voltage and calcium sensitivity of the protein in many species (4, 8, 18, 26, 31). To date, at least six splice sites have been characterized in the coding region of the mouse transcript, and the beginning of the transcript,

including the start of the open reading frame, has been shown to be highly diverse (Ref. 8; Fig. 5A). To assess the distribution of mSlo1 splice variants in the parotid gland, the coding region for the COOH terminus of the protein, where most of the identified splice sites occur, was amplified using RT-PCR and multiple clones were sequenced. All of the clones were found to be identical and insertless at each of the characterized splice sites. Additional 5'-RACE and RT-PCR of the full-length clone suggested that a single mSlo1 transcript was expressed in the parotid gland (data not shown). This transcript corresponded to a short version of the protein, resulting from an in-frame stop codon following the final splice site. This splice variant is highly homologous to the human Slo1 mRNA (accession no. NM_002247) and differs primarily in the last eight conceptually translated amino acids, as shown in Fig. 5B.

We compared several properties of the mouse parotid mSlo variant (parSlo) expressed in CHO and HEK cells with the time- and voltage-dependent current in native parotid cells. Figure 1, *bottom inset*, contains an example of single-channel currents in an inside-out patch from a HEK cell transfected with the parSlo. The single-channel current-voltage relationship of parSlo channels expressed in HEK (Fig. 1, open circles) and CHO cells (Fig. 1, open inverted triangles) was similar to that of the large-conductance channels in the native cells.

Maxi-K channels are sensitive to the scorpion toxins CTX and IBX (13). Expressed IK1 channels are also sensitive to CTX but are relatively insensitive to IBX (15, 36). Thus IBX is a specific pharmacological tool for maxi-K channels, so we examined IBX block of native

currents and recombinantly-expressed mSlo channels. Figure 6A, *inset*, contains an example of the time- and voltage-dependent currents of native parotid acinar cells recorded in the presence of 300 nM clotrimazole to minimize mIK1 channel activity. The main part of Fig. 6A shows that application of 500 nM IBX had a modest effect on the current recorded at +50 mV. In this example, 500 nM IBX blocked ~33% of the current. The average amount of block of native current by this concentration was $38 \pm 2.1\%$ ($n = 6$).

Heterologously expressed parSlo produced time- and voltage-dependent currents (Fig. 6B, *inset*) that were generally similar to the currents in native cells. However, though not investigated in detail, the time course of activation of expressed parSlo was somewhat faster than the current in the native cells. Significantly, expressed parSlo channels were considerably more sensitive to IBX than the native current. The main part of Fig. 6B shows that 100 nM IBX blocked 95% of the current (at +50 mV) through parSlo channels heterologously expressed in CHO cells. Similar data with 2–100 nM IBX were fit by a standard binding isotherm with an EC₅₀ value of 6.1 ± 2 nM for IBX block of homomeric parSlo channels expressed in HEK cells.

The good agreement between the single-channel conductance coupled with the discrepancy between the IBX sensitivity of the native current and expressed parSlo raises the possibility that the native channels may contain an auxiliary subunit in addition to the product of the parSlo gene. Four β -subunits that can assemble with Slo proteins have been identified (3, 6, 9, 10, 24, 35), and the presence of these β -subunits alters

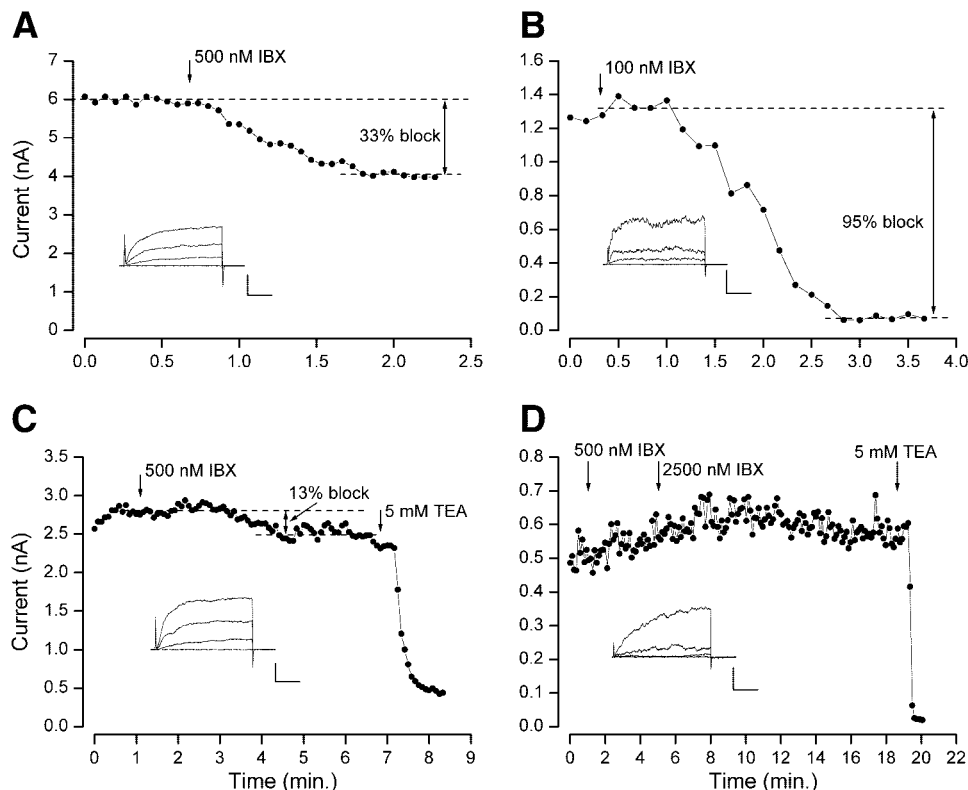


Fig. 6. Iberitoxin block of parotid and expressed K⁺ channels. *A*: native parotid acinar cells treated with 300 nM clotrimazole to minimize mIK1 channel activity. Current was activated by 160 nM intracellular Ca²⁺. Current was measured at the end of pulses to +50 mV. Application of 500 nM iberitoxin (IBX) is indicated by the arrow. *B*: data from a cell transfected with parSlo only. Application of 100 nM IBX is indicated by the arrow. *C*: data from a cell cotransfected with parSlo+ β ₁. Applications of 500 nM IBX and 5 mM TEA are indicated by arrows. *D*: data from an HEK cell cotransfected with parSlo+ β ₄. Applications of 500 and 2,500 nM IBX and 5 mM TEA are indicated by arrows. All currents (except those in *A*) are from CHO cells patched with 400 nM Ca²⁺. *Insets*: raw currents in response to steps of membrane voltage to +10, +30, and +50 mV. Calibrations: 2 nA, 10 ms (*A*); 0.5 nA, 10 ms (*B*); 1 nA, 10 ms (*C*); 0.25 nA, 20 ms (*D*).

the scorpion toxin sensitivity of the heteromeric channels (3, 10, 24).

To test for the presence of these β -subunits in the mouse parotid gland, we designed primer pairs for RT-PCR analysis based on multiple sequence alignments of the published β -subunit gene products (human *KCNMB1-4*; mouse *Kcnmb1* and *4*). The following goals applied: first, to flank homologous segments of the β -subunit coding regions; second, to prevent cross-hybridization; and third, to end the primers on codons that represent highly conserved amino acids. This strategy was expected to yield primer pairs for β_2 - and β_3 -subunits that would recognize both the human and mouse homologs, because the mouse cDNA sequences had yet to be reported. Our results indicated that β_1 - and β_4 -subunits were most prominently expressed in mouse parotid gland, whereas the β_2 and β_3 amplicon sets could be validated for use in mice by using mouse kidney and trachea cDNA templates, respectively (Fig. 7). Furthermore, successive rounds of amplification failed to result in the accumulation of specific PCR products for β_2 - or β_3 -subunits from parotid cDNA, suggesting that their expression levels are below the detection limits of our assay (data not shown).

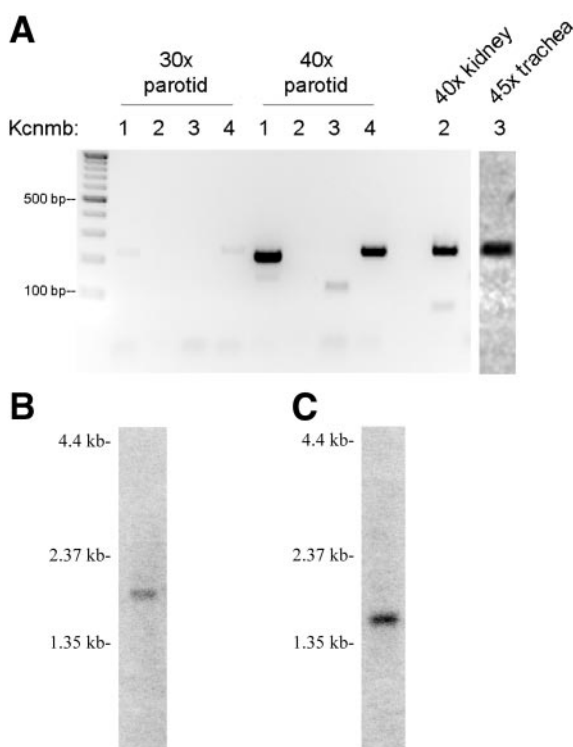


Fig. 7. Expression of mSlo β -subunits 1–4 (*Kcnmb1-4* genes) in the parotid gland. A: RT-PCR was used to amplify mouse parotid gland cDNA with oligonucleotide pairs specific for the mouse large-conductance Ca²⁺-activated K⁺ channel β -subunit isoforms 1–4 for the indicated number of cycles. β_1 and β_4 were expressed in the mouse parotid gland, whereas β_2 and β_3 were not. Control reactions indicated that β_2 was expressed in the mouse kidney and β_3 was expressed in the trachea. B: Northern blot of parotid mRNA hybridized to a probe for maxi-K β_1 . The probe detected a single band of ~ 1.7 kb. C: Northern blot of parotid mRNA hybridized to a probe for maxi-K β_4 . This probe hybridized with an mRNA of ~ 1.45 kb.

Expression of the β_1 - and β_4 -subunit mRNA in parotid gland was demonstrated directly by Northern blot analysis (Fig. 7B). We used a commercially available anti- β_1 antibody but were unable to detect a specific signal in a preparation of parotid gland membranes by Western blot analysis (data not shown). Similarly, attempts to localize the signal to specific cells in the parotid gland through immunohistochemistry were unsuccessful. Thus molecular studies alone cannot determine which of the two β -subunits, if either, are expressed in parotid acinar cells. To answer this question, we compared the electrophysiological and pharmacological characteristics of the parSlo channel coexpressed with either β_1 or β_4 to the endogenous parotid acinar cell current.

Heteromeric parSlo+ β_1 channels expressed voltage- and time-dependent currents (Fig. 6C, inset) generally similar to the currents in native cells. These heteromeric channels had a single-channel conductance indistinguishable from that of homomeric parSlo channels (not shown) consistent with results with hSlo and the human β_1 -subunit (27). However, the addition of the β_1 -subunit substantially reduced the IBX sensitivity of the channels, as shown in the main part of Fig. 6C. Even 500 nM IBX had only a modest effect on heteromeric parSlo+ β_1 : an average block at +50 mV of $17.5 \pm 7\%$ ($n = 5$). This degree of block is consistent with an EC₅₀ value of 2,400 nM, and in agreement with this value, 2,500 nM blocked 54 and 47% of the current in two independent experiments. Heteromeric parSlo+ β_1 channels remained sensitive to external TEA, as shown in Fig. 6C.

Coexpression of parSlo and β_4 also produced time- and voltage-dependent currents resembling those in the native cells (Fig. 6D, inset) with the same single-channel conductance as the native channels and homomeric parSlo channels expressed in HEK and CHO cells (data not shown). As shown in the main part of Fig. 6D, heteromeric parSlo+ β_4 channels were entirely insensitive to 500 nM IBX. This concentration of toxin reduced the current (at +50 mV) through the heteromeric channels expressed in CHO cells by $1.9 \pm 1.6\%$ ($n = 3$). Application of 2,500 nM for >10 min (Fig. 6D) had no more effect than 500 nM ($P > 0.1$, $n = 3$). As shown, these heteromeric parSlo+ β_4 channels remained sensitive to external TEA.

Thus the voltage- and time-dependent current in mouse parotid acinar cells did not have the IBX sensitivity of homomeric parSlo channels or that of heteromeric parSlo+ β_1 or β_4 channels, raising the possibility that the native current could include two populations of channels: one that is relatively sensitive to the toxin (like homomeric parSlo channels), and one that is toxin resistant (like heteromeric parSlo+ β_1 or β_4 channels). The data in Fig. 8A show that only $\sim 39\%$ of the native current (in BlackSwiss \times 129/SvJ mice) was sensitive to IBX. This IBX-sensitive component had an EC₅₀ value of $\sim 31 \pm 14$ nM. About 61% of the voltage- and time-dependent current in mouse parotid acinar cells was insensitive to IBX up to concentrations as large as 2,500 nM. We also examined the CTX sensitivity of the

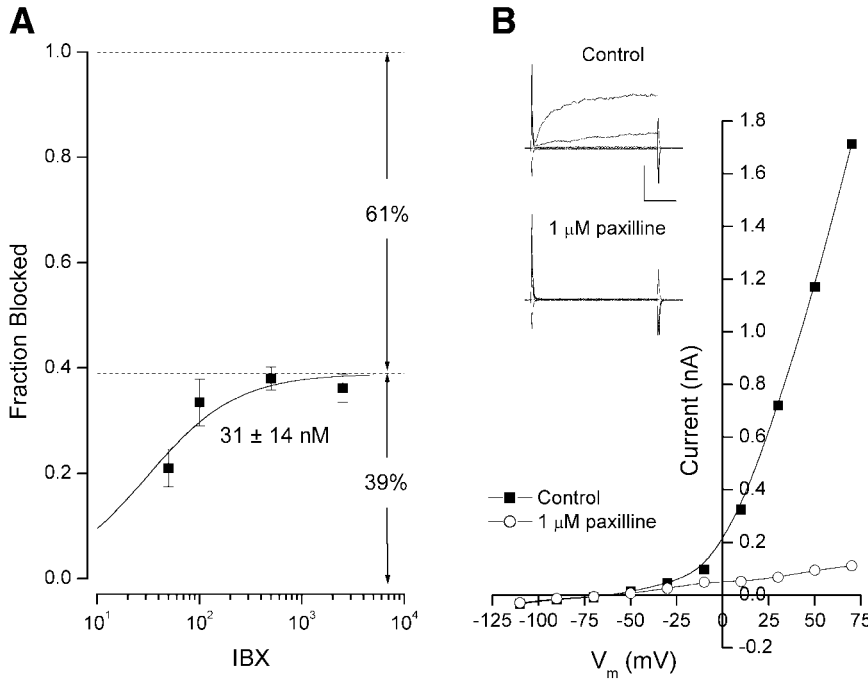


Fig. 8. IBX and paxilline block of maxi-K channels in mouse parotid acinar cells. *A*: concentration dependence of the amount of block of parotid acinar cell currents by the indicated concentrations of IBX. Ca²⁺-activated current induced by 160 nM Ca²⁺ (except for 1 experiment with 250 nM). The time- and voltage-insensitive current was minimized by application of 300 nM clotrimazole. Values are means ± SE from 3–6 measurements. Line represents fit of a standard binding isotherm with EC₅₀ and maximum block values of 31 ± 14 nM and 39 ± 3.2%, respectively. *B*: paxilline block of maxi-K channels in mouse parotid acinar cells. Currents were measured at the end of 40-ms pulses to the voltages indicated from a -70-mV holding potential in the absence (control) and presence of 1 μM paxilline. *Inset*: raw currents from 40-ms steps to membrane potentials of -110, -30, 10, and 50 mV from a holding voltage of -70 mV in the absence (control) and presence of 1 μM paxilline as indicated.

channels in native cells and found that 55 ± 2% of the current was sensitive to this toxin with an EC₅₀ value of 13 ± 2 nM (data not shown); ~45% of the current was insensitive to CTX up to levels as high as 500 nM.

Even though only 40–45% of the native time-, voltage-, and Ca²⁺-dependent current was sensitive to even very high IBX and CTX concentrations, much, if not all, of the current could be blocked by external TEA, as shown in Fig. 6, *C* and *D*. In addition, essentially all the current could be inhibited by paxilline. This diterpene mycotoxin is a very potent nonpetidyl inhibitor of maxi-K channels (reviewed in Ref. 13). In the example in Fig. 8*B*, 1 μM paxilline blocked 96% of the time- and voltage-dependent current in the presence of 160 nM intracellular Ca²⁺ (and 300 nM clotrimazole to inhibit current through mIK1 channels). The average inhibition in five such experiments was 94 ± 1.9%. This result and those with external TEA indicate that 100% of the current recorded with these conditions is through maxi-K channels even though not all the current can be blocked by even very high concentrations of the scorpion toxins.

The moderate sensitivity of heteromeric parSlo+β₁ channels to IBX (see Fig. 6*C* and related text above) suggests that these channels do not contribute significantly to the total maxi-K current in native parotid acinar cells. However, the slow onset and small block of the heterologously expressed heteromeric channels diminishes the strength of any such conclusion. An alternate method to test the idea that heteromeric parSlo+β₁ channels do not contribute significantly to the maxi-K current in native cells is to determine the IBX sensitivity of the current in cells from mice in which the β₁ gene has been disrupted (7). The results of such a test are presented in Fig. 9.

Figure 9 shows the amount of IBX block of maxi-K channels in β₁ knockout mice (filled squares) along with similar data from their wild-type counterparts (open circles). There appears to be little difference between the IBX block of wild-type and β₁ knockout

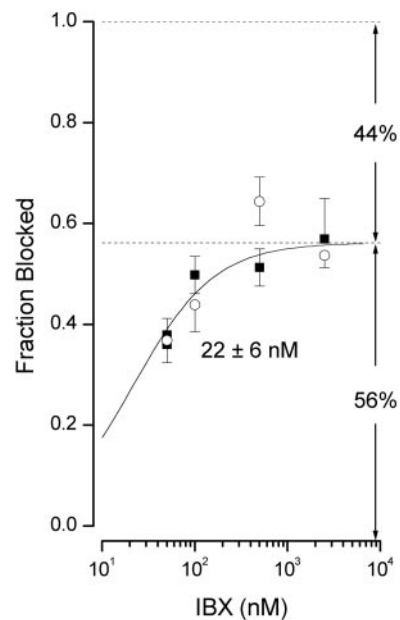


Fig. 9. IBX block of maxi-K channels from β₁ knockout mice. Concentration dependence of the amount of block of parotid acinar cell currents by the indicated concentrations of IBX is shown. Ca²⁺-activated current induced by 160 nM Ca²⁺. The time- and voltage-insensitive current was minimized by application of 300 nM clotrimazole. Values are means ± SE from 3–4 measurements. Data are from C57BL/6J (○) and β₁ knockout animals (■). Line represents fit of a standard binding isotherm with EC₅₀ and maximum block values of 22 ± 6 nM and 56 ± 2%, respectively.

animals, and all the data are consistent with $56 \pm 2\%$ of the current sensitive to IBX with an EC₅₀ value of 22 ± 6 nM; that is, there is $\sim 50\%$ of the maxi-K current in mouse parotid that is insensitive to IBX whether or not the β_1 gene is active, confirming the suggestion that heteromeric parSlo+ β_1 channels do not significantly contribute to the maxi-K current of mouse parotid acinar cells.

DISCUSSION

There have been multiple studies of K⁺ channels in several types of salivary glands from different species (12, 14, 16, 22, 29). The results of these various studies suggest that the K⁺ channel expression pattern may be specific to particular glands and particular species. Therefore, a complete understanding of the physiological role of K⁺ channels in salivary glands requires a systematic approach that includes identifying the relevant genes in a single model system as well as a quantitative comparison of the electrophysiological properties of the native channels with those of expressed, candidate genes.

Developments in targeted gene ablation technology have made the mouse an attractive system in which to examine the physiological role of ion transport proteins in transmembrane fluid dynamics (25). We found that mouse parotid acinar cells express significant amount of only two types of Ca²⁺-activated K⁺ channels: 1) a relatively time- and voltage-independent K-selective channel that has a single-channel conductance (in 135 mM external K⁺) of ~ 22 pS, and 2) a voltage- and time-dependent K⁺ channel with a single-channel conductance of ~ 140 pS. These properties suggested *Kcnn4* (mIK1) and *Kcnma* (mSlo) as candidate genes coding for these channels. Thus we designed experiments to determine whether these genes were expressed in mouse parotid acinar cells and compared several properties of the native channels with those of the heterologously expressed candidate genes.

Northern blot and in situ analyses showed that mIK1 was abundantly expressed in acinar but not ductal cells of the mouse parotid gland, consistent with a primary role in secretion in this tissue. This finding is consistent with the observation that salivary glands express the highest detectable levels of mIK1 transcript among all of the organs surveyed (16). Other sources of mIK1 include nonexcitable tissues such as lung, trachea, kidney, and stomach. The distribution of mIK1 in tissues rich in epithelia supports a significant role for mIK1 in secretion or electrolyte reabsorption.

Heterologously expressed mIK1 channels have several properties in common with the voltage- and time-independent K⁺ current in mouse parotid acinar cells: 1) a single-channel conductance indistinguishable from that of the native current, 2) a similar lack of voltage and time dependence, 3) a similar sensitivity to clotrimazole, and 4) a nearly identical sensitivity to TEA.

Because the voltage- and time-dependent component of K⁺ current in the native cells appeared to have the properties of a maxi-K channel, we tested for the ex-

pression of genes known to code for these types of channels. The gene family to which Slo1, the original maxi-K channel, belongs is composed of two additional members, Slo2 and Slo3. As expected on the basis of their published distribution (mSlo3 is testes specific) and activities (mSlo2 is chloride dependent; mSlo3 is pH sensitive/Ca²⁺ insensitive), the results of RT-PCR analysis suggest that mSlo1 is the most prominently expressed member of this gene family in the parotid gland.

The mSlo1 gene has been shown to have alternatively spliced products, and many of the splice variants exhibit distinct electrophysiological characteristics and greatly differing Ca²⁺ sensitivities (4, 8, 18, 31). We assayed the most common splice sites in the NH₂ and COOH termini of the protein and found that a single homogenous insertless variant was present in the parotid gland. Although this variant has previously been described in mice (31), it has not been assayed electrophysiologically. Instead, a separate variant, mbr5 (8), was expressed for patch-clamp analysis under the assumption that it was insertless (31). However, the mbr5 variant contains a three-amino acid insertion (IYF) at the second splice site in the COOH terminus and, in addition, codes for the "long" form of the protein. The true insertless form of mSlo ends prematurely because of a cryptic stop codon brought into frame by the splicing of nucleotides 3408–3436 from the mSlo coding region. Interestingly, the insertless mSlo variant found in the parotid most closely resembles one of the published human Slo sequence variants (11, 27, 33).

The mouse parotid mSlo variant (parSlo) expressed in HEK and CHO cells had a single-channel conductance that was indistinguishable from the large-conductance channel in the native cells. However, heterologously expressed parSlo channels were substantially more sensitive to IBX than was the current in the native cells. Thus we tested for the presence of four mSlo β -subunits known to alter scorpion toxin sensitivity. We found that the mouse parotid expressed only the β_1 - and β_4 -subunits, and we examined the IBX sensitivity of parSlo coexpressed with each of these subunits.

We found that both the mouse β_1 - and β_4 -subunits reduce the IBX sensitivity of the mouse parotid mSlo variant parSlo, with a larger effect produced by the β_4 -subunit: heteromeric parSlo+ β_4 channels were insensitive to IBX concentrations as large as 2,500 nM. This is the first examination of the actions of IBX on this particular mSlo splice variant in heteromeric channels with the mouse β -subunits, so no direct comparison to existing data is possible. However, our results are qualitatively similar to those obtained with human Slo (hSlo) channels coexpressed with human β_1 - and β_4 -subunits (3, 10, 24), although the coassembly of the mouse parotid mSlo variant with the β -subunits appears to more substantially decrease IBX sensitivity.

We found that the IBX and CTX dose-response relationships of the native channels (Figs. 8A and 9) were consistent with two populations of maxi-K type chan-

nels in the native cells: one (~50% of the total) with a reasonably high affinity for toxin, and another population that is essentially insensitive to the toxin (to 500 nM CTX and 2,500 nM IBX). Because we found heteromeric parSlo+ β_1 channels to be moderately sensitive to IBX and hSlo+ β_1 are quite CTX sensitive (3, 24), it seems reasonable to consider that the maxi-K, Ca²⁺-activated K⁺ current in native parotid is composed of approximately equal numbers of homotetrameric parSlo channels and heteromeric parSlo+ β_4 channels. This suggestion is strengthened by our results showing that ~50% of the maxi-K current in parotid acinar cells from β_1 knockout mice remained insensitive to 2,500 nM IBX. Although the β_1 gene ablation results could be compromised by an exact compensation by β_4 expression, the most parsimonious explanation that accounts for all the data is that mouse parotid acinar cells express equal numbers of homotetrameric parSlo channels and heteromeric parSlo+ β_4 channels.

We thank Keerang Park for cloning the mK1 from mouse parotid tissue and Paul D. Kingsley for assistance with the in situ analysis. We are grateful to J. E. Melvin for considerable discussions of this work and for critically reading the manuscript. We thank J. Thompson for assistance with the electrophysiological experiments and for critically reading the manuscript and Jodi Pilato and Pamela McPherson for the preparation of parotid acinar cells.

This work was supported by National Institute of Dental Research Grants DE-13539 (T. Begenisich) and DE-14119 (K. Nehrke).

REFERENCES

- Arreola J, Melvin JE, and Begenisich T. Activation of calcium-dependent chloride channels in rat parotid acinar cells. *J Gen Physiol* 108: 35–47, 1996.
- Atkinson NS, Robertson GA, and Ganetzky B. A component of calcium-activated potassium channels encoded by the *Drosophila slo* locus. *Science* 253: 551–555, 1991.
- Behrens R, Nolting A, Reimann F, Schwarz M, Waldschütz R, and Pongs O. hKCNMB3 and hKCNMB4, cloning and characterization of two members of the large-conductance calcium-activated potassium channel β subunit family. *FEBS Lett* 474: 99–106, 2000.
- Benkusky NA, Fergus DJ, Zuccherro TM, and England SK. Regulation of the Ca²⁺-sensitive domains of the maxi-K channel in the mouse myometrium during gestation. *J Biol Chem* 275: 27712–27719, 2000.
- Bers D, Patton C, and Nuccitelli R. A practical guide to the preparation of Ca buffers. *Methods Cell Biol* 40:3–29, 1994.
- Brenner R, Jegla TJ, Wickenden A, Liu Y, and Aldrich RW. Cloning and functional characterization of novel large conductance calcium-activated potassium channel β subunits, hKCNMB3 and hKCNMB4. *J Biol Chem* 275: 6453–6461, 2000.
- Brenner R, Perez GJ, Bonev AD, Eckman D, Kosek JC, Willer SW, Patterson AJ, Nelson MT, and Aldrich RW. Vasoregulation by the β_1 subunit of the calcium-activated potassium channel. *Nature* 407:870–876, 2000.
- Butler A, Tsunoda S, McCobb DP, Wei A, and Salkoff L. mSlo, a complex mouse gene encoding “maxi” calcium-activated potassium channels. *Science* 261: 221–224, 1993.
- Chang CP, Dworetzky SI, Wang J, and Goldstein ME. Differential expression of the α and β subunits of the large-conductance calcium-activated potassium channel: implications for channel diversity. *Mol Brain Res* 45: 33–40, 1997.
- Dworetzky SI, Boissard CG, Lum-Ragan JT, McKay MC, Post-Munson DJ, Trojnecki JT, Chang CP, and Gribkoff VK. Phenotypic alteration of a human BK (*hSlo*) channel by *hSlo β* subunit coexpression: changes in blocker sensitivity, activation/relaxation and inactivation kinetics, and protein kinase A modulation. *J Neurosci* 16:4543–4550, 1996.
- Dworetzky SI, Trojnecki JT, and Gribkoff VK. Cloning and expression of a human large-conductance calcium-activated potassium channel. *Mol Brain Res* 27: 189–193, 1994.
- Gallacher DV and Morris AP. A patch-clamp study of potassium currents in resting acetylcholine-stimulated mouse submandibular acinar cells. *J Physiol* 373: 379–395, 1986.
- Gribkoff VK, Starrett JE Jr, and Dworetzky SI. The pharmacology and molecular biology of large-conductance calcium-activated (BK) potassium channels. *Adv Pharmacol* 17: 319–348, 1997.
- Hayashi T, Young JA, and Cook DI. The Ach-evoked Ca²⁺-activated K⁺ current in mouse mandibular secretory cells. Single channel studies. *J Membr Biol* 151: 19–27, 1996.
- Ishii TM, Silvia C, Hirschberg B, Bond CT, Adelman JP, and Maylie J. A human intermediate conductance calcium-activated potassium channel. *Proc Natl Acad Sci USA* 94: 11651–11656, 1997.
- Ishikawa T and Murakami M. Tetraethylammonium-insensitive, Ca²⁺-activated whole-cell K⁺ currents in rat submandibular acinar cells. *Pflügers Arch* 428: 516–525, 1995.
- Jensen BS, Strobaek D, Christophersen P, Jorgensen TD, Hansen C, Silahtaroglu A, Olesen SP, and Ahring PK. Characterization of the cloned human intermediate-conductance Ca²⁺-activated K⁺ channel. *Am J Physiol Cell Physiol* 275: C848–C856, 1998.
- Lagrutta A, Shen KZ, North RA, and Adelman JP. Functional differences among alternatively spliced variants of Slowpoke, a *Drosophila* calcium-activated potassium channel. *J Biol Chem* 269: 20347–20351, 1994.
- Lau KR, Howorth AJ, and Case RM. Identification and regulation of K⁺ and Cl⁻ channels in human parotid acinar cells. *J Physiol* 425: 407–427, 1990.
- Logsdon NJ, Kang J, Togo JA, Christian EP, and Aiyar J. A novel gene, *hKCa4*, encodes the calcium-activated potassium channel in human T lymphocytes. *J Biol Chem* 272: 32723–32726, 1997.
- Martinez JR, Cassity N, and Reed P. An examination of functional linkage between K efflux and ³⁶Cl efflux in rat submandibular gland in vitro. *Arch Oral Biol* 32: 891–895, 1987.
- Maruyama Y, Gallacher DV, and Petersen OH. Voltage and Ca²⁺-activated K⁺ channel in basolateral acinar cell membranes in mammalian salivary glands. *Nature* 302: 827–829, 1983.
- Maruyama Y, Nishiyama A, and Teshima T. Two types of cation channels in the basolateral cell membrane of human salivary gland acinar cells. *Jpn J Physiol* 36: 219–223, 1986.
- Meera P, Wallner M, and Toro L. A neuronal β subunit (KCNMB4) makes the large conductance, voltage- and Ca²⁺-activated K⁺ channel resistant to charybdotoxin and iberiotoxin. *Proc Natl Acad Sci USA* 97: 5562–5567, 2000.
- Melvin JE, Nguyen HV, Evans RL, and Shull GE. What can transgenic and gene targeted mouse models teach us about salivary gland physiology? *Adv Dent Res* 14: 5–11, 2000.
- Navaratnam DS, Bell TJ, Tu TD, Cohen EL, and Oberholtzer JC. Differential distribution of Ca²⁺-activated K⁺ channel splice variants among hair cells along the tonotopic axis of the chick cochlea. *Neuron* 19: 1077–1085, 1997.
- Pallanck L and Ganetzky B. Cloning and characterization of human and mouse homologs of the *Drosophila* calcium-activated potassium channel gene, slowpoke. *Hum Mol Genet* 3: 1239–1243, 1994.
- Park CS, Hausdorff SF, and Miller C. Design, synthesis, and functional expression of a gene for charybdotoxin, a peptide blocker of K⁺ channels. *Proc Natl Acad Sci USA* 88: 2046–2050, 1991.
- Park K, Case RM, and Brown PD. Identification and regulation of K⁺ and Cl⁻ channels in human parotid acinar cells. *Arch Oral Biol* 46: 801–810, 2001.
- Schreiber M, Wei A, Yuan A, Gaut J, Saito M, and Salkoff L. Slo3, a novel pH-sensitive K⁺ channel from mammalian spermatocytes. *J Biol Chem* 273: 3509–3516, 1998.
- Shipston MJ, Duncan RR, Clark AG, Antoni FA, and Tian L. Molecular components of large conductance calcium-activated potassium (BK) channels in mouse pituitary corticotropes. *Mol Endocrinol* 13: 1728–1737, 1999.

32. **Stampe P, Kolmakova-Partensky L, and Miller C.** Intimations of K⁺ channel structure from a complete functional map of the molecular surface of charybdotoxin. *Biochemistry* 33:443–450.
33. **Tseng-Crank J, Foster CD, Krause JD, Mertz R, Godinot N, DiChiara TJ, and Reinhart PH.** Cloning, expression, and distribution of functionally distinct Ca²⁺-activated K⁺ channel isoforms from human brain. *Neuron* 13: 1315–1330, 1994.
34. **Turner RJ, George JN, and Baum BJ.** Evidence for a Na⁺/K⁺/Cl⁻ cotransport system in basolateral membrane vesicles from the rabbit parotid. *J Membr Biol* 94: 143–152, 1986.
35. **Uebele VN, Lagrutta A, Wade T, Figueroa DJ, Liu Y, McKenna E, Austin CP, Bennett PB, and Swanson R.** Cloning and functional expression of two families of β -subunits of the large-conductance calcium-activated K⁺ channel. *J Biol Chem* 275: 23211–23218, 2000.
36. **Vandorpe DH, Shmukler BE, Jiang L, Lim B, Maylie J, Adelman JP, de Franceschi L, Cappellini MD, Brugnara C, and Alper SL.** cDNA cloning and functional expression of the mouse Ca²⁺-gated channel, mIK1. *J Biol Chem* 273: 21542–21553, 1998.
37. **Warth R, Hamm K, Bleich M, Kunzelmann K, von Hahn T, Scrieber R, Ullrich E, Mengel M, Trautmann N, Kindle P, Schwab A, and Greger R.** Molecular and functional characterization of the Ca²⁺-regulated K⁺ channel (rSK4) of colonic crypts. *Pflügers Arch* 438: 437–444, 1999.
38. **Wilkinson DG and Green J.** *Postimplantation Mammalian Embryos: A Practical Approach*, edited by Copp AJ and Cockcroft DL. New York: Oxford University Press, 1990, p. 155–171.
39. **Wulff H, Miller MJ, Hansel W, Grissmer S, Cahalan MD, and Chandry KG.** Design of a potent and selective inhibitor of the intermediate-conductance Ca²⁺-activated K⁺ channel, IKCa1: a potent immunosuppressant. *Proc Natl Acad Sci USA* 97: 8151–8156, 2000.
40. **Yuan A, Dourado M, Butler A, Walton N, Wei A, and Salkoff L.** SLO-2, a K⁺ channel with an unusual Cl⁻ dependence. *Nat Neurosci* 3: 771–779, 2000.

